An investigation of some Schiff base derivatives as chemosensors for Zn(II): The performance characteristics and potential applications

Ece Ergun [a*], Ümit Ergun [b], Özgür İleri [b], Muhammed Fatih Küçükmüzevir [b]

[*] corresponding author
e-mail:ece.ergun@taek.gov.tr
phone:+90.312.8101591
fax:+90.312.8154307

[a] TAEA, Sarayköy Nuclear Research and Training Center, Kazan, 06983, Ankara, Turkey
[b] Department of Chemistry, Faculty of Art and Sciences, Düzce University, Düzce 81620, Turkey

Abstract

The fluorescence properties of four simple Schiff bases (LH_2, $LDMH_2$, LH_2^H and LDM^HH_2) and their potential application as chemosensors for the detection of zinc ion in aqueous solution have been investigated. While LH_2 and $LDMH_2$ have displayed specific recognition to Zn(II), the reduced derivatives (LH_2^H and LDM^HH_2) of these ligands have shown no fluorescence response due to the lack of C=N group. The Job plots, fluorescence titration experiments and ESI-MS results indicate the formation of 1:1 complexes between sensors and Zn(II). The analytic methods based on LH_2 and $LDMH_2$ as chemosensors have been proposed and optimized to detect Zn(II) ions in aqueous solution. The optimized methods have shown a good range of linearity**,** high precision, good accuracy and low detection limit. As an alternative to these methods, LH_2 and $LDMH_2$ have the capability to detect Zn(II) ions by naked eye under UV lamp. Moreover, LH_2-Zn and $LDMH_2$-Zn complexes have the ability to be a staining agent for identifying the radiation treatment of food by DNA comet assay.

Keywords: Zinc ion; Chemosensor; Fluorescent probe; Schiff bases; Aqueous solution

1. Introduction

Zinc is one of the most common element in the Earth' crust. Zinc is found in the air, soil and water and is present in all foods [1]. Zinc concentrations, however, are rising unnaturally, due to anthropogenic additions. Most zinc is added during industrial activities, such as mining, coal, and waste combustion and steel processing. Industrial sources or toxic waste sites may cause the concentrations of Zn(II) in drinking water to reach levels that can cause health problems [2]. Zinc is an essential trace element in biological systems and has been found to play an important role in survival and functioning of all living organisms. It is only second to iron among the trace elements found in humans [3]. In total, the adult human body contains 2–3 g zinc. Probably thousands of proteins contain zinc and over 200 zinc-containing enzymes have now been characterized [4]. Zinc can be relatively easily determined by standard analytical techniques such as AAS or ICP-MS, but the determination of the "free" or "available" Zn(II) concentrations in some samples such as biological systems has proved difficult using classic techniques. So, this has led to the emergence of zinc specific molecular sensors.

Among the various chemosensors, fluorescent chemosensors present many advantages, which are high sensitivity, low cost, easy detection, and suitability as a diagnostic tool for ion recognition and biological concern [5, 6, 7, 8, 9]. Because Zn(II) is spectroscopically silent due to its d10 electron configuration, numerical fluorescent chemosensors for the detection of Zn(II) have been studied intensively [10-16]. The nitrogen of a Schiff base exhibits a strong affinity for zinc, therefore, the Schiff base has also been used to develop zinc chemosensors [10, 17-24]. It has been reported that two mechanisms, the C=N isomerization and the suppression of this isomerization, are responsible for fluorescence emission behavior of the Schiff bases [10, 17, 22]. The binding of metal ions by the C=N group would stop the isomerization, and a significant fluorescence enhancement could be achieved. However, the main drawbacks of Schiff-base type receptors are the poor solubility and the instability of the Schiff-base in aqueous solutions. In addition, many available fluorescent chemosensors for Zn(II) encountered difficulty in distinguishing Zn(II) from other metal ions (especially from

Cd(II), Ni(II) and Cu(II)), because of their similar properties or paramagnetic nature [11-15, 18, 20, 22-25]. Most of these chemosensors have been used particularly for live-cell imaging because interfering ions are present in much lower concentrations compared with Zn(II) in biological samples. However, it is important to testify the potential use of the chemosensors for the monitoring of Zn(II) concentrations in water samples containing significant amounts of heavy metal ions. Besides, the synthesis of some chemosensors requires complicated pathways which can be time-consuming with low yields and costly.

Contamination of foods, especially of those of animal origin, with microorganisms, particularly pathogenic non-spore-forming bacteria, parasitic helminths and protozoa is an enormous public health problem and important cause of human suffering all over the world. Considering the tremendous importance of microbial and parasitic diseases related to foods, food safety should be guaranteed. The chemical sanitizing procedures have inherent problems concerning residues and environmental pollution. This is where food irradiation among the other intervention alternatives comes into the picture [26]. A number of analytical methods have been investigated for the detection of radiation treatment of foods. In 1996, the European Committee for Standardization (CEN) adapted several methods based on Electron Spin Resonance (ESR) spectroscopy, Gas Chromatography (GC) and Thermoluminescence (TL). Since all these techniques for the detection of irradiated foods are expensive, time consuming and need special expertise, therefore, there is a need to find out rapid and simple tests, which should be versatile and require inexpensive instrumentation. Since the large molecule of DNA is a sensitive target to ionizing radiation, radiation-induced changes in DNA could be a basis for detection of irradiation in a number of foods. A sensitive technique to detect DNA fragmentation is the microgel electrophoresis of single cells, commonly called 'Comet Assay' [27].

DNA Comet Assay has been described as a rapid and inexpensive screening test to identify radiation treatment of food. This method involves lysis with detergent and high salt, after embedding cells in agarose so that the DNA is immobilized for subsequent electrophoresis. The DNA fragments migrate out of the cells during the electrophoresis, forming a long 'tail' in the direction of the anode and giving the damaged cells the appearance of a comet. In contrast, non-irradiated DNA samples appear as discrete dots on the gel, lacking a 'tail' or with only slight 'tails'. The most common way to visualize the comets is staining with a fluorescent dye such as ethidium bromide, DAPI, acridine orange and propidium iodide and then examining by a fluorescent microscope [28-30]. At this point, the fluorescent compounds in our study have been investigated for their potentiality as DNA staining agents.

In this study, two symmetric ONNO type Schiff base N-N'-bis(salicylidene)-1,3-propanediamine (LH_2), bis-N,N'-(salicylidene)-2,2'-dimethyl-1,3-propanediamine ($LDMH_2$), and the reduced derivatives (LH_2^H and LDM^HH_2) of this Schiff bases (Fig. 1) have been synthesized and examined for their potential use as fluorescent chemosensors for the detection of Zn(II) in water. These are not novel ligands but will provide convenience and flexibility for researchers who need to analyze zinc due to their simple synthesis and even the commercial availability of one (LH_2). Fluorescence is known to be very sensitive to the environment, so the parameters which play an important role in regulating the fluorescent property of the studied compounds have also been optimized. The results show that LH_2 and $LDMH_2$ are highly selective and sensitive probes for Zn(II) in aqueous solution.

2. Experimental section

2.1. Reagents and apparatus

All chemicals were obtained commercially (analytical grade and spectroscopic grade) and used without further purification. Absorption spectra were obtained by an Agilent Cary 100 UV-Vis spectrophotometer. Fluorescence spectra measurements were performed on a Cary Eclipse fluorescence spectrophotometer. The pH values were determined using a Mettler Toledo pH probe. Electrospray ionization mass spectra (ESI-MS) were carried out on a Waters Micromass ZQ 2000 spectrometer.

2.2. Synthesis of chemosensors

Bis-N,N'-(salicylidene)-1,3-propanediamine (LH_2), bis-N,N'-(salicylidene)-2,2'-dimethyl-1,3-propanediamine ($LDMH_2$), bis-N,N'-(2-hydroxybenzyl)-1,3-propanediamine (L^HH_2), and bis-N,N'-(2-hydroxybenzyl)-2,2'-dimethyl-1,3-propanediamine (LDM^HH_2) were prepared according to the reported procedure [31, 32]. According to the procedure, LH_2 and $LDMH_2$ were prepared by the condensation of salicylaldehyde with 1,3-diaminopropane and 2,2'-dimethyl-1,3-propanediamine in ethanol, respectively. After the isolation, these Schiff bases were reduced with sodium borohydride to obtain L^HH_2 and LDM^HH_2.

2.3. Spectroscopic studies

The stock solutions of chemosensors (LH_2, $LDMH_2$, L^HH_2 and LDM^HH_2) (2.0×10^{-3} M) were prepared in ethanol. Stock solutions (2.0×10^{-3} M) of Fe(III), Al(III), Cr(III), Mn(II), Cd(II), Co(II), Cu(II), Ni(II), Pb(II), Hg(II), Ca(II), Mg(II), K(I), Na(I) and Zn(II) were prepared from their nitrate or chloride salts in deionized water. Spectral data were recorded at room temperature. For fluorescence measurements, both the excitation and emission slit widths were 5.0 nm unless otherwise stated.

ESI-MS studies were performed in the positive ion mode with a quadrupole mass analyzer. The major conditions were as follows: scan range, m/z 50–800; capillary voltage, 3.5kV; cone voltage, 30V; source temperature, 150 °C; desolvation temperature, 300 °C.

2.4. Irradiation and DNA comet assay

The gamma irradiation of chicken breast meat samples was carried out in a Co-60 laboratory irradiator (Ob-Servo Sanguis**,** Institute of Isotopes, Hu), at dose of 3.00 kGy (dose rate 1.83 kGy/h) at Saraykoy Nuclear Research and Training Center. The effect of gamma-ray radiation on DNA in chicken breast was examined by DNA comet assay. The DNA Comet Assay for the cell suspensions was carried out as described in the European Standard EN 13784 [33]. The coated slides were immersed in lysis buffer (0.045MTBE, pH 8.4, containing 2.5% SDS) for 7 min. Using the same buffer but devoid of SDS, electrophoresis (Thermo Electrophoresis System) was performed at 2 V/cm for 2 min. The mixtures of LH_2-Zn and $LDMH_2$-Zn ([L] = 1×10^{-4}, [Zn] = 1×10^{-4}) was employed as staining agent to visualize DNA in irradiated and non-irradiated samples. Slides were examined using a microscope (Olympus BX51 model with fluorescence, DIC attachments and filter U-DM-DA/FI/TX2E) at magnification 20×(Objective) by digital color video camera (Penguin PIXERA 600 CL).

3. Results and Discussion

3.1. UV–vis and fluorescence studies of chemosensors with various metal ions

UV–Vis absorption spectra of LH_2 and L^HH_2 (1.0×10^{-5} M in ethanol) are shown in Fig. 2a. It is known that the isolated benzene ring exhibits three characteristic π-π* absorption bands; two primary bands at 184 and 202 nm and a secondary band at 255 nm. However, these bands shift to longer wavelengths depending on the nature of the substituents, i.e. their electron donating or withdrawing nature [34]. Schiff bases, in this study, contain two benzene ring, however, absorption bands of the benzene are expected to be somewhat red-shifted in the UV spectra of these ligands due to the substitution. This can be easily observed in UV-Vis spectrum of L^HH_2 (Fig. 2a), which exhibits only three absorption bands of benzene (201, 218 as a shoulder, and 281 nm) that are red-shifted compared to isolated benzene. On the other hand, in the case of an electron-withdrawing group substitution such as C=N, the primary absorption bands are shifted to a longer wavelengths (especially second primary band), but the position of secondary absorption band does not significantly change [34]. These effects can be seen in the spectrum of LH_2; two primary bands were shifted to longer wavelengths (216 and 257 nm) compared to the bands obtained in L^HH_2 spectrum and the position of secondary absorption band did not significantly change (282 nm). Another difference observed in the electronic spectrum of LH_2 was associated with the appearance of two new bands at 320 and 405 nm due to the presence of azomethine group. These bands were attributed to the π-π* and n-π* transitions of the C=N chromophore. It should be noted that $LDMH_2$ and LDM^HH_2 ligands, containing only two additional methyl groups compared to LH_2 and L^HH_2, gave similar absorption spectra (data not shown).

The binding ability of the ligands in ethanol (2.0×10^{-5} M) with cations in deionized water (2.0×10^{-3} M), such as Na(I), K(I), Mg(II), Ca(II), Al(III), Cr(III), Mn(II), Fe(III), Co(II), Ni(II), Cu(II), Zn(II), Cd(II) and Pb(II), was examined. Upon addition of Na(I), K(I), Mg(II), Ca(II), Al(III), Cr(III), Mn(II), Fe(III), Cd(II) and Pb(II) no significant changes in absorption bands were observed (the inset of Fig. 2b). By contrast, addition of Co(II), Ni(II), Cu(II) and Zn(II) resulted in a redshift of C=N band indicating the formation of metal complexes (Fig. 2b). It should be indicated that in all ligands studied, π-π* transitions of benzene exhibit maximum absorption at the same wavelength but somewhat broadened. $LDMH_2$ has showed similar binding affinity toward the ions mentioned above, therefore, only the absorption spectra of LH_2 and LH_2-cation mixtures are given in Fig. 2b to illustrate these interactions. On the other hand, since the binding affinity is determined by the redshift of the C=N band, it is not possible to observe a change in the spectra of L^HH_2 and LDM^HH_2 due to the absence of this bond.

The complexation of LH_2 and $LDMH_2$ with Co(II), Ni(II), Cu(II) and Zn(II) ions was monitored using UV–visible spectrophotometric studies. The absorption spectra shown in Fig. S1, depict the spectral changes upon titrating a fixed concentration of LH_2 and $LDMH_2$ (1.0×10^{-4} M) against increasing concentrations of Zn^{2+} ions (0–1.0×10^{-4} M) in ethanol:water = 1:1 (v/v). It is noteworthy that, the intensity of π-π* transition of the C=N chromophore gradually increased along with redshift on increasing the concentrations of Co(II), Ni(II), Cu(II) and Zn(II) ions. In addition, the intensity of absorbance bands corresponding to the n-π* transition also decreased, indicating ligands coordinate to the metal ions through azomethine nitrogen. The appearance of clear isosbestic points suggests that an equilibrium was established between ligands and metal ions.

Fluorescence studies were further performed in order to evaluate the potential use of the ligands as fluorescent chemosensors for identification of metal ions. First, preliminary emission spectra were scanned to find emission peak wavelength of free ligands in ethanol (1.0×10^{-5} M), ligand-deionized water (1:1 v/v, stock ligand solution in ethanol 2.0×10^{-5} M)

and ligand-cation (stock cation solution in water 2.0×10^{-3} M) mixtures (1:1 v/v). As can be seen in Fig. 3a and b, free LH_2 and $LDMH_2$ emitted only one fluorescence peak appeared at 446 and 451 nm, respectively. The excitation spectra obtained from emission at 446 and 451 nm for LH_2 and $LDMH_2$ gave three peaks (the insets of Fig. 3a and b) at 235, 268, 349 nm (LH_2) and 238, 271, 356 nm ($LDMH_2$). On the other hand, no emission peak was observed for the reduced ligands (data not shown). This result is an evidence that the C=N bond is required for fluorescence emission of these ligands. Upon the addition of deionized water to LH_2 and $LDMH_2$ solutions (2.0×10^{-5} M) in ethanol (1:1, v/v), the observed emission band decreased, probably due to decrease in solubility of ligands, increase in solvent polarity and hydrolysis of carbon-nitrogen double bond (Fig. 3a and b). These suggestion were examined by UV-Vis studies (Fig. S2). It was observed that UV-Vis spectra of ligands in ethanol and in ethanol:water (1:1) mixture showed different absorption characteristics. In ethanol:water mixture, the intensity of π-π* transitions were decreased while the intensity of n-π* transition was increased accompanied with a blue shift (λ_{max}=410 nm in ethanol; λ_{max}=400 nm in ethanol:water) (the inset of Fig. S2a and S2b). It is known that position (λ_{max}) and intensity (ε_{max}) of the absorption bands are affected by the surrounding molecular environment due to the intermolecular interactions and/or change in solubility. Therefore, the spectral modifications mentioned above appeared as a result of change in solvent composition. Consequently, the decrease in intensity of π-π* absorptions in ethanol:water environment resulted in a decrease in fluorescence emission of the ligands. Another factor that contributed the observed decrease in intensity can be the hydrolysis of the ligands. It is well known that Schiff bases undergo hydrolysis in acidic, neutral and basic conditions by different rate limiting pathways [35, 36]. The spectral studies clearly indicated that intensity of π-π* transition of the C=N chromophore decreased accompanied with a redshift for a definite period of time after mixing the ligand solutions in ethanol with water (Fig. S2a and S2b). It can be suggested that the observed decrease occurs because of the hydrolysis of ligands by the attack of H_2O to the imine linkage. In addition, the increase in solvent polarity (due to the presence of water) decreases the energy of π-π* transitions. Therefore, the observed redshift in the absorption maxima in a time range (0-40 min for LH_2, Fig. S2a; 0-120 min for $LDMH_2$, Fig. S2b) was the result of this phenomenon. Furthermore, hydrolysis reaction caused also a decrease in the intensity of n-π* absorption over the same period of time. As the result of hydrolysis reaction, the lone pair of nitrogen becomes a bonding pair and C=N double bond content is reduced. So, less intense n-π* absorption bands were detected as time progressed. At this point, it is considered that hydrogen bonding also plays an important role. The presence of water enhanced the number of hydrogen bonds, leading an increase in the energy of n-π* transitions and absorption maximum appeared blue shifted over the definite time range mentioned above. As a consequence, it can be suggested that all mentioned interactions modify position, intensity and shape of absorption bands, resulting in a decrease in the intensity of fluorescence emission of the ligands in ethanol:water media. For better elucidation, effect of hydrolysis was examined by mass spectrometry studies and obtained results are given in Section 3.4.

The fluorescence responses of LH_2 and $LDMH_2$ with the common metal ions were investigated to evaluate whether these ligands could serve as a cation-selective chemosensor. Interestingly, a significant fluorescence emission was observed only for Zn(II) and Al(III) upon the treatment with LH_2 and $LDMH_2$. These peaks appeared at 446 nm for Zn(II) and at 484 nm for Al(III) in the emission scan spectra of both ligands (Fig. 4). In order to determine the best excitation wavelength for Zn(II)-ligand solutions, the emission wavelength was fixed at 446 nm. The most symmetrical and ideal gaussian-shape excitation peak was obtained at

350 nm for both LH_2 and $LDMH_2$, so this wavelength was used as the excitation wavelength during analysis.

On the other hand, no significant fluorescence emission was observed when LH_2 and $LDMH_2$ were treated with other cations (Fig. 4). In particular, the absence of any significant peak in the emission scan spectra of the ligands treated with Co(II), Ni(II), Cu(II) and Cd(II), the most frequently described as interfering ions for Zn(II) sensing in the literature, is one of the most remarkable result at this point. In addition, the red shift of Al(III)-ligand emission peak compared with Zn(II)-ligand peak will allow the fluorometric determination of Zn(II) without any significant interference (selectivity of ligands to zinc ion over other metal ions were investigated in Section 3.5). Finally, the reduced derivatives ($L^{H}H_2$ and $LDM^{H}H_2$) did not give any fluorescence signal even with Zn(II) as expected (data not shown). Therefore, it should be noted that further optimization studies were performed with LH_2 and $LDMH_2$.

The fluorescence associated with the reaction of ligands with Zn(II) can readily detectable under a UV lamp. Under 365 nm UV light, a bright fluorescence was clearly visible to naked eyes only for LH_2-Zn^{2+} and $LDMH_2$-Zn^{2+} solutions, whereas no significant fluorescence could be observed for the ligand solutions with other metal ions (Fig. 5). This feature is useful for the fast visual Zn(II) detection.

The observed fluorescence enhancement was attributed to occurrence of the strong complexation via addition of Zn(II) to LH_2 and $LDMH_2$ ligands (Fig. S3). Based on the obtained results it can be suggested that the complexation of ligands with Zn(II) makes the Schiff bases more rigid, restricts the C=N isomerization, prevents the rapid hydrolysis and produces a large chelation-enhanced fluorescence (CHEF) effect [37]. However, although complex formation in Co(II)-ligand, Ni(II)-ligand, Cu(II)-ligand and Cd(II)-ligand solutions was detected by UV-Vis spectrometer, these complexes did not exhibit fluorescence emission. This can be explained by electron occupancy of d orbitals of the metal ions. Usually transition metals with partially filled d-orbital often quench the fluorescence of the fluorophore through a highly efficient non-radiative pathway while transition metals like Zn(II) with fully filled d-orbital do not possess any low energy metal centered orbitals and hence such charge transfer through non radiative pathway is prohibited [38-40].

3.2. Optimization studies

The parameters such as solvent, ligand concentration, pH, response time and stability of ligand-metal complexes, and presence of interfering ions were optimized to achieve the best fluorescence performance for the studied compounds.

3.2.1. Solvent effect

It is well known that the solvents play significant role in the optical properties of ligand-metal complexes. In order to describe the fluorescence emission behavior of the LH_2-Zn and $LDMH_2$-Zn complexes in different solvents, ligands were dissolved in ethanol, methanol, acetonitrile, acetone, N,N dimethylformamide (DMF), dimethyl sulfoxide (DMSO), and isopropanol (2×10^{-5} M). The fluorescence scan spectra were recorded after mixing these ligand solutions with Zn(II) solution (1:1 v/v, stock $[Zn^{2+}] = 2.0\times10^{-3}$ M in water), respectively. The fluorescence emission was observed with all of the above mentioned solvents for the ligands in the presence of Zn(II). It was obtained that although the change in wavelength of excitation and emission was not pronounced, different solvents showed

enhancing and quenching effect on the emission intensity. As can be seen in Fig. 6 there was a significant enhancement in the fluorescence intensity by addition of Zn(II) to the ethanol, DMF and DMSO solutions of LH_2 and $LDMH_2$. Taking into account of the economic cost, practical application, and environmental factors subsequent experiments were carried out with the ligands dissolved in ethanol.

3.2.2. Ligand concentration

It is known that there is an equilibrium between the chemosensor/analyte in free form and the chemosensor-analyte complex. An increase in the ligand concentration will drive this equilibrium reaction to the right, which can lead to an improvement in fluorescence signal. Therefore, fresh LH_2 and $LDMH_2$ solutions, each at 2.0×10^{-4} and 2.0×10^{-3} M concentrations, were prepared in ethanol in order to examine the fluorescence response. After adding Zn(II) solution (2.0×10^{-3} M in water) to each sensor solution (1:1 v/v), fluorescence spectra were recorded (λ_{Ex} = 350 nm). It was observed that addition of 2.0×10^{-3} M Zn(II) to 2.0×10^{-4} M ligand solutions caused fluorescence enhancement approximately 2.5 fold for LH_2 and 2 fold for $LDMH_2$ compared to the signals obtained from 2.0×10^{-5} M ligand-2.0×10^{-3} M Zn(II) mixtures. On the other hand, after about 20 minutes following the addition of 2.0×10^{-3} M Zn(II) to 2.0×10^{-3} M LH_2, a white precipitate was observed. Such precipitation was observed after 3 days for $LDMH_2$-Zn mixture at same concentrations, however, in much lower amounts. Under this conditions, 2.0×10^{-4} M ligand solutions were used in further studies.

3.2.3. Response time and stability

In this study, response time is defined as the time at which the complex formation reaction reaches an equilibrium and the detected fluorescence signal becomes almost constant. Fig. 7 shows the fluorescence intensities of LH_2-Zn and $LDMH_2$-Zn complexes versus time at different detection intervals. As can be seen in Fig. 7a the fluorescence intensity of LH_2-Zn showed a substantial increase over the time interval from 0 min to 30 min following mixing of 2.0×10^{-4} M ligand and 2.0×10^{-3} M zinc solutions. On the other hand, a much slower fluorescence increase was observed in 2.0×10^{-4} M $LDMH_2$ and 2.0×10^{-3} M Zn(II) mixture (Fig. 7b), indicating that $LDMH_2$-Zn complex formation was slower than LH_2-Zn formation. However, the fluorescence response of the LH_2-Zn complex began to decrease after 60 minutes, while the fluorescence intensity of the $LDMH_2$-Zn complex remained almost constant after about 270th minute until 2 days. This result indicates that the interaction of Zn(II) with $LDMH_2$ forms a complex with much more stable fluorescent response than LH_2-Zn. Nevertheless, it should be pointed out that a decrease in fluorescence intensity of $LDMH_2$-Zn complex was also observed after 2 days. This study was repeated with the solutions prepared by lower zinc concentration (2.0×10^{-5} M) than the ligand concentration (2.0×10^{-4} M) and similar results were obtained (Fig. 7).

The decrease in the fluorescence response of LH_2-Zn complex can be explained by the alterations in its molecular structure. It has been reported that the versatile coordination properties of the Zn(II) ion allow for a large variety of structures ranging from monomers to oligomers or polymers and networks resulting from the self-assembly of Zn(II) with polydentate ligands [41]. Such changes in chemical composition over time can quench the fluorescence property or cause shifts in the absorption and emission maxima of LH_2-Zn, which results in a decrease in the emission at 446 nm. On the other hand, the decrease in fluorescence response of $LDMH_2$-Zn complex was observed after a very long time (after 2

days). This result may be attributed to the flexibility of the backbone. Since 2,2'-dimethyl-1,3-propanediamine is less flexible than 1,3-diaminopropane, the structural changes mentioned above may take place over a long time span. As a result, it is more convenient to perform zinc analysis within 30-60 minutes after the addition of LH_2, however, $LDMH_2$ and zinc mixture should be left for approximately 5 hours prior to take the spectrum.

3.2.4. pH effect

The effect of pH on the fluorescence response was investigated to determine a suitable pH condition for Zn(II) detection. For this purpose, a series of zinc solutions (blank, 2.0×10^{-3} M, 2.0×10^{-4} M and 2.0×10^{-5} M) each with a pH of 2-9 were prepared as representatives of Zn(II) samples with different concentrations. The pH of the solutions was not adjusted to values above 9 in order to avoid the precipitation of $Zn(OH)_2$ totally. After the ligand solutions (2.0×10^{-4} M) were added to these solutions, fluorescence spectra were recorded (λ_{Ex} = 350 nm) after 45 minutes for LH_2 and 5 hours for $LDMH_2$ (Fig. 8).

No significant change in the fluorescence emission intensity of the blank solutions (ligand-water) was observed in the mentioned pH range, indicating that Zn(II)-free ligand solutions are pH-insensitive. However, in presence of all concentrations of Zn(II), solutions had a very weak fluorescence response in the acidic environment (pH 4-5) due to protonation [42]. Protonation of active sites on the ligands inhibits their coordination with metals. It should be indicated that no fluorescence emission was obtained in strong acid medium (pH 2-4), probably due to acidic decomposition of the Schiff base complexes. This suggestion was examined by ESI-MS and the results were reported in Section 3.4. As the pH increased (pH 5-6), a gradual increase in fluorescence intensity was observed because of deprotonation. However, a decrease in fluorescence intensity occurred when the pH value exceeded 7, which can be explained by the onset of the formation of the colloidal $Zn(OH)_2$ species. It is worth noting that the largest fluorescence enhancement was achieved at about pH 7. Since pH value of Zn(II)-ligand solutions is about 7 after mixing, Zn(II) can be detected by using LH_2 and $LDMH_2$ without pH adjustment or buffering. This finding has some important outcomes, such as reducing the time and chemical consumption and improving the practical application of the method.

3.3. Job's plot, fluorescence titration and binding constant

In order to determine the stoichiometry of LH_2-Zn and $LDMH_2$-Zn complexes, the Job's plots were obtained by the fluorescence method. The intensity of fluorescence emission was measured by varying the mole fraction of Zn(II) (the ratio of Zn(II) and ligands varies in increments from 0:10 up to 10:0). As shown in Fig. 9a and 9b, the fluorescence emission intensity showed a maximum when the molar fractions of Zn(II) were very close to 0.5 for both ligands. These results demonstrates the formation of 1:1ratio of ligands with Zn(II).

For better elucidation of the binding mode of ligands with Zn(II), fluorescence titration experiments were performed. As clearly shown, increasing the concentration of Zn(II) results in a gradual increase in the fluorescence intensity of LH_2 (1×10^{-4} M) and $LDMH_2$ (0.5×10^{-4} M) until saturation is achieved (Fig. S4). The saturation of $1x10^{-4}$ M LH_2 and $0.5x10^{-4}$ M $LDMH_2$, evident in Fig. S4, has occurred almost with the same Zn(II) concentrations, which corresponds to a 1:1 interaction. However, the exact position of the saturation point was determined by linear regression equations obtained from the linear sections of the saturated and non-saturated part of the curve (Fig. S4). The x-positions of the sections (corresponding

to the Zn(II) concentrations at which saturation occurs) were calculated to be 0.91×10^{-4} M for LH_2-Zn and 0.47×10^{-4} M for $LDMH_2$-Zn titration curves (Eq. S1), which is in good agreement with the 1:1 interaction. Based on the fluorescence titration experiments, the binding constants of 1:1 LH_2-Zn and $LDMH_2$-Zn complexes were calculated by Benesi–Hildebrand plots and found to be 1.02×10^{4} M^{-1} and 3.96×10^{4} M^{-1}, respectively (Fig. S5, Eq. S2).

To further confirm the binding stoichiometry of ligands with Zn(II), ESI-MS experiments were also carried out (Section 3.4).

3.4. ESI-MS binding studies

Electrospray ionization mass spectrometry (ESI-MS) was used to characterize the ligand-metal binding properties. The ESI-MS spectra of LH_2 and $LDMH_2$ in ethanol (Fig. 10a and 10e) were dominated by the $[M+H]^+$ ions at m/z 283 and 311 that corresponds to the molecular weight of the Schiff bases. The peaks at m/z 305 (Fig. 10a) and m/z 333 (Fig. 10e) were identified as the sodium adduct ions.

As mentioned in Section 3.1, the decrease in fluorescence intensity observed in ligand-water mixtures was also examined by mass spectrometer. It was found that both ligands underwent hydrolysis when they were mixed with DI water. As can be seen in Fig. 10b and 10f, intensities of the molecular ion peaks of the ligands are relatively low and new ions are observed in ESI-MS spectra, corresponding to hydrolysis products of the ligands. The ions at m/z 179 (Fig. 10b) and m/z 207 (Fig. 10f) were assigned to $[C_{10}H_{15}N_2O]^+$ for LH_2 and $[C_{12}H_{19}N_2O]^+$ for $LDMH_2$, respectively. It is proposed that these ions are generated by loss of a hydrolysis product (salicylaldehyde) from the ligand structure. The ions at m/z 136, 107, 75 and 58, observed for both ligands, were attributed to $[C_8H_{10}NO]^+$, $[C_7H_7O]^+$, $[C_3H_{11}N_2]^+$ and $[C_3H_8N]^+$, respectively. The product ion at m/z 136 could be explained by loss of C_2H_5N (ethanimine) group from m/z 179 and elimination of C_4H_9N (methallylamine) moiety from m/z 207. Loss of CH_3N (methenamine) group from m/z 136 led to the formation of an ion at m/z 107. The peak at m/z 75 was assigned to molecular ion peak of 1,3-propanediamine and direct elimination of NH_3 from this molecule gave the peak observed at m/z 58 (allylamine). It should be also indicated that the ion at m/z 103 was observed only in the spectra related to $LDMH_2$ and assigned to protonated N,N′-dimethyl-1,3-propanediamine. Although the ion at m/z 75 was attributed to protonated 1,3-propanediamine, this peak can be also seen in $LDMH_2$ spectra due to direct loss of etilen from m/z 103.

The mass spectra of the LH_2-Zn(II) and $LDMH_2$-Zn(II) show molecular ion peaks at m/z 345 and m/z 373, respectively (Fig. 10c and 10g). These peaks correspond to the molecular weight of the respective compounds and demonstrate that the binding ratio of ligands and Zn(II) is a 1:1 stoichiometry. These spectra also indicate that the ions of hydrolysis products are less pronounced, which means Zn(II)-ligand complexes are relatively stable towards hydrolysis and this coordination largely prevents premature ligand dissociation.

In Section 3.2.4, it was proposed that acidic decomposition occurred at pH 2-4. As can be seen in Fig. 10d and 10h, no peak corresponding to the metal complexes or protonated free ligands is observed, indicating these compounds were fully decomposed. The peaks found in the spectra were resulted from the fragmentation of the main compounds. The peak at m/z 121 was attributed to $[C_7H_5O_2]^+$ and produced by loss of a labile hydrogen atom from salicylaldehyde. The product ion at m/z 93 observed for both ligand-Zn complexes was

generated by elimination of CO group from m/z 121. The ion m/z 86, like the ion m/z 103, was found only in the mass spectrum associated with $LDMH_2$ and formed by the loss of NH_3 group from m/z 103. In addition to these ions, the ions at m/z 75 and 58 structural information of which were given above were also seen in the spectrum.

Finally, the decrease in fluorescence response observed for the LH_2-Zn complex solution after 60 minutes was mentioned in Section 3.2.3, and it was suggested that this decrease might be due to alterations in molecular structure over time. This suggestion was confirmed by ESI-MS studies and found that new peaks were appeared at m/z 690, 692 and 694 in the mass spectrum of LH_2-Zn solution after 60 minutes (data not shown). It should be also pointed out that intensity of these peaks were increased over time. The ions at m/z 690 $[M]^+$, 692 $[M+2]^+$ and 694 $[M+4]^+$ were indicative of new dimeric Zn(II) complex formation. Furthermore, the white precipitate obtained after the addition of 2.0×10^{-3} M Zn(II) to 2.0×10^{-3} M LH_2 (Section 3.2.2) probably occurred due to the formation such dimeric or oligomeric etc. structures.

3.5. Selectivity of ligands to zinc ion over other metal ions

The selectivity of LH_2 and $LDMH_2$ for Zn(II) over other metal ions, such as Na(I), K(I), Mg(II), Ca(II), Al(III), Cr(III), Mn(II), Hg(II), Fe(III), Co(II), Ni(II), Cu(II), Cd(II) and Pb(II), was investigated. Based on the data obtained from the optimization studies, firstly each ion (2×10^{-3} M, in water) was added to zinc solution (2×10^{-4} M, in ethanol) (1:1, v/v) and then each metal ion solution was mixed with LH_2 and $LDMH_2$ (2×10^{-4} M) (1:1 v/v). The pH adjustment was not required because the pH of the solutions were in neutral conditions after mixing. Fluorescence spectra of these mixtures were recorded (λ_{Ex} = 350 nm) after 45 minutes for LH_2 and 5 hours for $LDMH_2$ and fluorescence intensity of each solution was given in Fig. 11. LH_2 and $LDMH_2$ were exhibited very good selectivity of zinc over other metals. While Al(III) ion slightly enhanced the fluorescence signal, Fe(III), Ni(II) and Cu(II) ions showed very little quenching effect. However, it should be noted that total interference of the metal ions had not practical significance when the fluorescence intensity of [Zn + all metal ions + L] was compared with that of [Zn + blank + L] solution.

The fluorescence response of the ligands toward individual metal ions has been previously discussed in Section 3.1. LH_2 and $LDMH_2$ have shown high selectivity for Zn(II) over other metal ions due to similar reasons such as close-shelled orbitals of zinc, appropriate ion radius, and binding affinity. It should be indicated that some metal ions such as Co(II), Ni(II), Cu(II) quenched the fluorescence significantly when the ligand concentrations were 1×10^{-5} M (data not shown). This can be explained by the fact that ligands have a higher affinity for these interfering cations than Zn(II) and probably only a small fraction of the ligand is available for binding to Zn(II) due to low ligand concentration. Thus, using a ligand at 1×10^{-4} M concentration does not only enhance the fluorescence response mentioned in Section 3.2.2, but also minimizes the quenching effect of certain cations by providing free ligand for Zn(II).

3.6. Analytical figures of merit

Under optimal conditions, individual calibration curves were constructed with several points for the determination of Zn(II). As shown in Fig. 12a, LH_2-Zn exhibited a linear response for the Zn(II) concentration range of $0.8 - 6.0\times10^{-5}$ M with correlation coefficient of $R^2 = 0.9992$ (n = 3). Limit of detection was calculated to be 0.5×10^{-6} M based on the definition by IUPAC (CDL = 3Sb/m, where Sb is the standard deviation from 10 blank solutions while m represents the slope of the calibration curve). On the other hand, the fluorescence response

observed for $LDMH_2$-Zn was linear for a wider range of Zn(II) concentrations ($0.3 - 5.0\times10^{-5}$ M, $R^2 = 0.9995$) compared to LH_2-Zn. Moreover, with a limit of detection down to 0.1×10^{-6} M, $LDMH_2$ was found to be more sensitive to Zn(II) ions at low concentrations than LH_2. For this reason, $LDMH_2$ is recommended as the preferred sensor for identification of low Zn(II) concentrations. In addition, the calibration curve of LH_2-Zn exhibited a saturation level beyond 8×10^{-5} M, so Zn(II) concentrations higher than 8×10^{-5} M could not be detected by using LH_2. However, the plateau observed for the Zn-$LDMH_2$ calibration curve originated from the fact that the fluorescence intensities of Zn(II) concentrations above 5×10^{-5} M were higher than the maximum setting value (1000 a.u) of the y-axis of the spectra. It should be indicated that linearity was obtained in the range of $7\times10^{-5} - 0.8\times10^{-5}$ M Zn (II) concentrations by reducing the emission slit width to 2.5 and creating a new calibration curve (the inset of Fig. 12b) based on this setting.

For the purpose of demonstrating the practical usefulness of the procedure, the analysis of Zn(II) in a certified ICP multielement (68 element) standard solution ICP-MS-68A was done by the proposed method under optimal conditions. Each metal concentration in this solution is 10 mg/L and standard is acidified with 2% HNO_3 to prevent hydrolysis of these metals. Therefore, appropriate dilutions were made to ensure that the Zn(II) concentration fell within the linear portion of the calibration curve and then pH of the sample was adjusted to approximately 7 (neutral pH). After the addition of LH_2 and $LDMH_2$ (2×10^{-4} M in ethanol, 1:1 v/v), samples were left for 45 minutes for LH_2 and 5 hours for $LDMH_2$ prior to take the spectrum. Fluorescence analysis of each sample was repeated 5 times (λ_{Ex} = 350 nm). The results were calculated by taking into account the dilution factor (Table 1).

In summary, according to the analytical performance parameters of the proposed method, LH_2 and $LDMH_2$ were adequate for the detection and quantification of Zn(II) in water samples, containing various cations. In this study, the sensitivity of the method is described in the terms of the limit of detection and the linearity evaluation experiments. With the methods based on LH_2 and $LDMH_2$ discussed above, sufficiently low LODs were achieved which allow the determination of low Zn(II) concentrations. The correlation coefficients (R^2) of the analytical curves were greater than 0.999, which is evidence of a fit of the data to the regression line. Since certified reference material was used, accuracy was expressed in terms of bias % in this study. It should be noted that proposed methods for both ligands provided bias less than 10%. The precision of the analyses was evaluated by determining the relative standard deviation (RSD %) under repeatability conditions and the methods based on both ligands were reported to be highly precise with an RSD of <1%.

3.7. DNA comet imaging

The effect of gamma-ray on DNA of chicken breast meat was examined by using a DNA comet assay. Fig. 1a and 1d show the color of LH_2-Zn and $LDMH_2$-Zn complexes, revealed as green under the microscope with U-DM-DA/FI/TX2E filter. After staining with LH_2-Zn and $LDMH_2$-Zn solutions and waiting at about 10 min, the non-irradiated and irradiated meat samples of chicken were clearly distinguishable just by naked eye inspection at the slide under the microscope as yellow-orange color (Fig 13b, 13c, 13e, 13f). Non-irradiated meat samples of chicken showed no comets because there was no DNA damage at 0.0 kGy as seen in Fig. 13b and 13e. In this assay, strand breaks of individual cells due to the gamma-ray irradiation at 3 kGy appear like tails of a comet (Fig. 13c and 13f). According to the obtained results, LH_2-Zn and $LDMH_2$-Zn solutions can serve as an alternative staining agent for identifying the radiation treatment of food by DNA comet assay. Future study will be focused

on the implementation of LH_2-Zn and $LDMH_2$-Zn complexes as staining agents on several food and biological samples. Moreover, fluorescence imaging experiments will be carried out in living cells.

4. Conclusion

In this study, four simple structure Schiff bases were synthesized and absorption, excitation and fluorescence properties of their zinc complexes were examined with the purpose of obtaining information about the usability of these ligands as a chemosensor for Zn(II) in aqueous solution. In conclusion, we successfully developed two "turn on" fluorescent chemosensors for the detection of Zn(II). The results obtained from this study suggest several important conclusions.

1. LH_2 and $LDMH_2$ showing good selectivity toward Zn(II) can be synthesized by a facile one-step Schiff base reaction, moreover LH_2 is commercially available. We think that this will provide a great convenience and flexibility to researchers who need to analyze zinc ion.

2. Although these are not new ligands, we have reported for the first time their applicability as fluorescent chemosensors. In addition, new methods have been developed for the rapid detection of Zn(II) using these ligands.

3. The important role of the C=N group in the fluorescent sensing mechanism has been demonstrated by studying with reduced derivatives of the ligands (L^HH_2 and LDM^HH_2).

4. The optimized method allows the determination of zinc in aqueous solutions. Zinc can be identified and quantified in aqueous neutral samples without pH adjustment.

5. The time required to reach the complex formation equilibrium is not very short (especially for $LDMH_2$-Zn), but most importantly, ligands are able to differentiate Zn^{2+} from other cations.

6. The optimized methods based on LH_2 and $LDMH_2$ show a good range of linearity, high precision, good accuracy and low detection limits.

7. These ligands can also be used as chemosensors for the detection of Zn(II) by the naked eye under UV lamp and thus allows for an extremely simple**,** rapid, and low-cost Zn(II) analysis by obviating the requirement of sophisticated equipments.

8. Beside the Zn(II) detection in water samples, LH_2-Zn and $LDMH_2$-Zn complexes offer an promising alternative as staining agent for identifying the radiation treatment of food by DNA comet assay.

Acknowledgements

We would like to thank Prof. Dr. Orhan Atakol for his guidance and support during ligand synthesis.

References

[1] S. Soni, A. Salhotra, M. Suar, Handbook of Research on Diverse Applications of Nanotechnology in Biomedicine, Chemistry, and Engineering. Chapter 24. Functionalized Magnetic Nanoparticles for Environmental Remediation, Sources of Heavy Metals in the Environment, IGI Global, (2015) p. 521.

[2] R.A. Wuana, F.E. Okieimen, Heavy Metals in Contaminated Soils: A Review of Sources, Chemistry, Risks and Best Available Strategies for Remediation, ISRN Ecol. 402647 (2011) 20 pages.
doi: 10.5402/2011/402647

[3] A. Dutta, Regulation of Zinc Homeostasis in Cultured Cells. Chapter 1. Introduction, ProQuest LLC, (2008) p. 1.

[4] N.C. Lim, H.C. Freake, C. Brückner, Illuminating Zinc in Biological Systems, Chem. Eur. J. 11 (2005) 38-49.
doi: 10.1002/chem.200400599

[5] Y. Guo, X. Tang, F. Hou, J. Wu, W. Dou, W. Qin, J. Ru, G. Zhang, W. Liu, X. Yao, A reversible fluorescent chemosensor for cyanide in 100% aqueous solution, Sens. Actuators B Chem. 181 (2013) 202-208.
http://dx.doi.org/10.1016/j.snb.2013.01.053

[6] Q. Lin, T.T. Lu, X. Zhu, T.B. Wei, H. Li, Y.M. Zhang, Rationally introduce multi-competitive binding interactions in supramolecular gels: a simple and efficient approach to develop multi-analyte sensor array, Chem. Sci. 7 (2016) 5341-5346.
http://dx.doi.org/10.1039/C6SC00955G

[7] Q. Lin, K.P. Zhong, J.H. Zhu, L. Ding, J.X. Su, H. Yao, T.B. Wei, Y.M. Zhang, Iodine Controlled Pillar[5]arene-Based Multiresponsive Supramolecular Polymer for Fluorescence Detection of Cyanide, Mercury, and Cysteine, Macromolecules 50 (2017) 7863-7871.
DOI: 10.1021/acs.macromol.7b01835

[8] Q. Lin, P.P. Mao, Y.Q. Fan, L. Liu, J. Liu, Y.M. Zhang, H. Yao, T.B. Wei, A novel supramolecular polymer gel based on naphthalimide functionalized-pillar[5]arene for the fluorescence detection of Hg^{2+} and I^- and recyclable removal of Hg^{2+} **via** cation–π interactions, Soft Matter 13 (2017) 7085-7089.
DOI: 10.1039/C7SM01447C

[9] Q. Lin, Y.Q. Fan, P.P. Mao, L. Liu, J. Liu, Y.M. Zhang, H. Yao, T.B. Wei, Pillar[5]arene-Based Supramolecular Organic Framework with Multi-Guest Detection and Recyclable Separation Properties, Chem. Eur. J. 24 (2018) 777-783.
DOI: 10.1002/chem.201705107

[10] Z. Xu, J. Yoon, D.R. Spring, Fluorescent chemosensors for Zn^{2+}, Chem Soc Rev. 39 (2010) 1996-2006.
doi: 10.1039/B916287A

[11] T. Liu, S. Liu, Responsive Polymers-Based Dual Fluorescent Chemosensors for Zn^{2+} Ions and Temperatures Working in Purely Aqueous Media, Anal. Chem. 83 (2011) (7) 2775-2785.
dx.doi.org/10.1021/ac200095f

[12] S.A. Ingale, F. Seela, A Ratiometric Fluorescent On–Off Zn^{2+} Chemosensor Based on a Tripropargylamine Pyrene Azide Click Adduct, J. Org. Chem. 77 (2012) 9352-9356. doi:10.1021/jo3014319

[13] Z. Mao, L. Hu, X. Dong, C. Zhong, B. Liu, Z. Liu, Highly Sensitive Quinoline-Based Two-Photon Fluorescent Probe for Monitoring Intracellular Free Zinc Ions, Anal. Chem. 86 (2014) 6548-6554.
doi: 10.1021/ac501947v

[14] Y. Tang, Y. Ding, X. Li, H. Ågren, T. Li, W. Zhang, Y. Xie, Acylation of dipyrromethanes at the α and β positions and further development of fluorescent Zn^{2+} probes, Sens. Actuators B Chem. 206 (2015) 291-302. http://dx.doi.org/10.1016/j.snb.2014.09.060

[15] H. Yu, T. Yu, M. Sun, J. Sun, S. Zhang, S. Wang, H. Jiang, A symmetric pseudo salen based turn-on fluorescent probe for sensitive detection and visual analysis of zinc ion, Talanta 125 (2014) 301-305.
http://dx.doi.org/10.1016/j.talanta.2014.03.011

[16] K. Akutsu, S. Mori, K. Shinmei, H. Iwase, Y. Nakano, Y. Fujii, Investigation of substitution effect on fluorescence properties of Zn^{2+}-selective ratiometric fluorescent compounds: 2-(2′-Hydroxyphenyl)benzimidazole derivatives, Talanta 146 (2016) 575-584.
http://dx.doi.org/10.1016/j.talanta.2015.09.001

[17] L. Li, Y. Dang, H. Li, B. Wang, Y. Wu, Fluorescent chemosensor based on Schiff base for selective detection of zinc(II) in aqueous solution, Tetrahedron Lett. 51 (2010) 618–621.
http://dx.doi.org/10.1016/j.tetlet.2009.11.070

[18] M. Hosseini, Z. Vaezi, M.R. Ganjali, F. Faridbod, S.D. Abkenar, K. Alizadeh, M. Salavati-Niasari, Fluorescence ″turn-on″ chemosensor for the selective detection of zinc ion based on Schiff-base derivative, Spectrochim. Acta Part A 75 (2010) 978-982.
http://dx.doi.org/10.1016/j.saa.2009.12.016

[19] M. Yan, T. Li, Z. Yang, A novel coumarin Schiff-base as a Zn(II) ion fluorescent sensor, Inorg. Chem. Commun. 14 (2011) 463-465.
doi:10.1016/j.inoche.2010.12.027

[20] K. Li, X. Wang, A. Tong. A “turn-on” fluorescent chemosensor for zinc ion with facile synthesis and application in live cell imaging, Anal. Chim. Acta 776 (2013) 69-73. http://dx.doi.org/10.1016/j.aca.2013.03.033

[21] N. Roy, H.A.R. Pramanik, P.C. Paul, S.T. Singh, A Sensitive Schiff-Base Fluorescent Chemosensor for the Selective Detection of $Zn^{2+,}$ J. Fluoresc. 24 (2014) 1099-1106. doi:10.1007/s10895-014-1390-3

[22] J. Yan, L. Fan, J. Qin, C. Li, Z. Yang, A novel and resumable Schiff-base fluorescent chemosensor for Zn(II), Tetrahedron Lett. 57 (2016) 2910-2914. http://dx.doi.org/10.1016/j.tetlet.2016.05.079

[23] V.K. Gupta, A.K. Singh, L.K. Kumawat, A turn-on fluorescent chemosensor for Zn^{2+} ions based on antipyrine schiff base, Sens. Actuators B Chem. 204 (2014) 507-514. http://dx.doi.org/10.1016/j.snb.2014.07.128

[24] Y. Li, K. Li, J. He. A "turn-on" fluorescent chemosensor for the detection of Zn(II) in aqueous solution at neutral pH and its application in live cells imaging, Talanta 153 (2016) 381-385.
http://dx.doi.org/10.1016/j.talanta.2016.03.040

[25] G.J. Park, J.J. Lee, G.R. You, L. Nguyen, I. Noh, C. Kim, A dual chemosensor for Zn^{2+} and Co^{2+} in aqueous media and living cells: Experimental and theoretical studies, Sens. Actuators B Chem. 223 (2016) 509-519.
http://dx.doi.org/10.1016/j.snb.2015.09.129

[26] J. Farkas, Irradiation as a method for decontaminating food. A review, Int. J. Food Microbiol. 1998 44(3):189-204.
https://doi.org/10.1016/S0168-1605(98)00132-9

[27] H.M. Khan, A.A. Khan, S. Khan, Application of DNA comet assay for detection of radiation treatment of grams and pulses, J. Food Sci. Technol. (2011) 48(6):718-723.
DOI 10.1007/s13197-010-0169-z

[28] Andrew R. Collins, The comet assay for DNA damage and repair: Principles, applications, and limitations, Mol. Biotechnol. (2004) 26: 249-261.
https://doi.org/10.1385/MB:26:3:249

[29] Y. Jo, B. Sanyal, K. Ameer, J.H. Kwon, Characterization of DNA comet and cellulose radical signal in Valencia oranges treated with different forms of ionizing radiation, Postharvest Biology and Technology 135 (2018) 68-76.
http://dx.doi.org/10.1016/j.postharvbio.2017.08.004

[30] T. Gichner, A. Mukherjee, J. Velemínský, DNA staining with the fluorochromes EtBr, DAPI and YOYO-1 in the comet assay with tobacco plants after treatment with ethyl methanesulphonate, hyperthermia and DNase-I, Mutat. Res. 605 (2006) 17-21.
doi:10.1016/j.mrgentox.2006.01.005

[31] S. Durmuş, Ü. Ergun, J.C. Jaud, K.C. Emregül, H. Fuess, O. Atakol, Thermal decomposition of some linear trinuclear Schiff base complexes with acetate bridges, J. Therm. Anal. Calorim. 86 (2006) 337–346.
https://doi.org/10.1007/s10973-005-7282-7

[32] B.M. Ateş, B. Zeybek, M. Aksu, Ü. Ergun, F. Ercan, M.L. Aksu, O. Atakol, Thermal decomposition of new mononuclear Ni^{II} complexes with ONNO type reduced Schiff bases and pseudo halogens, Z. Anorg. Allg. Chem. 636 (2010) 840−845. doi: 10.1002/zaac.200900499

[33] CEN, 2001. EN 13784 Foodstuffs – DNA Comet Assay for the Detection of Irradiated Foodstuffs – Screening Method. European Committee for Standardization, Brussles.

[34] D.L. Pavia, G.M. Lampman, G.S. Kriz, J.A. Vyvyan, Introduction to Spectroscopy. Chapter 10 Ultraviolet Spectroscopy, Cengage Learning, 5th edition, USA, (2014) p. 602.

[35] E.H. Cordes, W.P. Jencks, The mechanism of hydrolysis of Schiff bases derived from aliphatic amines, J. Am. Chem. Soc. 85 (1963) 2843-2848. DOI: 10.1021/ja00901a037

[36] A.C. Dash, B. Dash, P.K. Mahapatra, Hydrolysis of imines. Part 2. Kinetics and mechanism of hydrolysis of N-Salicylidene-2-aminopyridine in the presence and absence of copper (II) Ion. A study of the catalytic effect of some mixed-ligand complexes of copper (II), J. Chem. Soc., Dalton Trans. 8 (1983) 1503-1509. DOI: 10.1039/DT9830001503

[37] L. Yang, W. Zhu, M. Fang, Q. Zhang, C. Li, A new carbazole-based Schiff-base as fluorescent chemosensor for selective detection of Fe^{3+} and Cu^{2+}, Spectrochim. Acta Part A 109 (2013) 186-192. http://dx.doi.org/10.1016/j.saa.2013.02.043

[38] L. Wang, H. Li, D. Cao, A new photoresponsive coumarin-derived Schiff base: Chemosensor selectively for Al^{3+} and Fe^{3+} and fluorescence ″turn-on″ under room light, Sens. Actuators B Chem. 181 (2013) 749-755. http://dx.doi.org/10.1016/j.snb.2013.01.090

[39] D. Sarkar, A.K. Pramanik, T.K. Mondal, Coumarin based fluorescent 'turn-on' chemosensor for Zn^{2+}: An experimental and theoretical study, J. Lumin. 146 (2014) 480-485. http://dx.doi.org/10.1016/j.jlumin.2013.09.080

[40] J. Wu, W. Liu, X. Zhuang, F. Wang, P. Wang, S. Tao, X. Zhang, S. Wu, S. Lee, Fluorescence turn on of Coumarin derivatives by metal cations: A new signaling mechanism based on C=N isomerization, Org. Lett. 9 (2007) 33-36. doi:10.1021/ol062518z

[41] A. Erxleben, Structures and properties of Zn(II) coordination polymers, Coord. Chem. Rev. 246 (2003) 203-228. http://dx.doi.org/10.1016/S0010-8545(03)00117-6

[42] A.A. El-Sherif, M.S. Aljahdali, Review: protonation, complex-formation equilibria, and metal–ligand interaction of salicylaldehyde Schiff bases, J. Coord. Chem. 66 (2013) 3423-3468. http://dx.doi.org/10.1080/00958972.2013.839027

Figure Captions

Fig. 1. Molecular structure of a) N-N'-bis(salicylidene)-1,3-propanediamine (LH_2), b) bis-N,N'-(salicylidene)-2,2'-dimethyl-1,3-propanediamine ($LDMH_2$), c) bis-N,N'-(2-hydroxybenzyl)-1,3-propanediamine (L^HH_2), d) bis-N,N'-(2-hydroxybenzyl)-2,2'-dimethyl-1,3-propanediamine (LDM^HH_2)

Fig. 2. UV–Vis spectra of a) LH_2 (1.0×10^{-5} M in ethanol) and L^HH_2 (1.0×10^{-5} M in ethanol) b) LH_2 (1.0×10^{-5} M in ethanol) and LH_2-cation mixtures (1:1 v/v, stock $[LH_2] = 2.0\times10^{-5}$ M in ethanol, stock [cation] = 2.0×10^{-3} M in DI water)

Fig. 3. Fluorescence excitation (inset) and emission spectra of a) LH_2 (1.0×10^{-5} M in ethanol) and LH_2-DI water mixture (1:1 v/v, stock $[LH_2] = 2.0\times10^{-5}$ M in ethanol) b) $LDMH_2$ (1.0×10^{-5} M in ethanol) and $LDMH_2$-DI water mixture (1:1 v/v, stock $[LDMH_2] = 2.0\times10^{-5}$ M in ethanol)

Fig 4. Fluorescence emission spectra of LH_2 and $LDMH_2$ (inset) in the presence of different cations (1:1 v/v, stock [ligand] = 2.0×10^{-5} M in ethanol, stock [cation] = 2.0×10^{-3} M in DI water)

Fig 5. Photographs of a) LH_2 and b) $LDMH_2$ with various metal ions under UV light (λ_{Ex} = 365 nm).

Fig. 6. Fluorescence intensity changes of LH_2 and $LDMH_2$ (1.0×10^{-5} M) in presence of Zn^{2+} (1.0×10^{-3} M) in different solvents: 1- ethanol; 2- methanol; 3- acetonitrile; 4- acetone; 5-DMF; 6- DMSO; 7- isopropanol at room temperature, respectively

Fig. 7. The influence of response time on the fluorescent intensity of a) LH_2 b) $LDMH_2$ in the presence of Zn(II) (1:1 v/v, stock $[LH_2] = [LDMH_2] = 2.0\times10^{-4}$ M in ethanol, stock $[Zn^{2+}] = 2.0\times10^{-3}$ M in DI water) (λ_{Ex} = 350 nm)

Fig. 8. The influence of pH on the fluorescent intensity of LH_2 and $LDMH_2$ in the presence of Zn(II) (1:1 v/v, stock $[LH_2] = [LDMH_2] = 2.0\times10^{-4}$ M in ethanol, stock $[Zn^{2+}] = 2.0\times10^{-5}$ M in DI water) (λ_{Ex} = 350 nm)

Fig. 9. Job's plot data for evaluating the stoichiometry of a) LH_2-Zn and b) $LDMH_2$-Zn complexes. The total concentrations of LH_2+Zn(II) and $LDMH_2$+Zn(II) were kept at 1.0×10^{-4} M and 0.5×10^{-4} M, respectively (λ_{Ex} = 350 nm)

Fig. 10. ESI-MS spectra of a) LH_2 in ethanol (1.0×10^{-4} M) b) LH_2 in ethanol + DI water mixture (1:1, v/v) c) LH_2 in the presence of 1 equiv. Zn(II) pH ≅ 7 d) LH_2 in the presence of 1 equiv. Zn(II) pH = 3 e) $LDMH_2$ in ethanol (1.0×10^{-4} M) f) $LDMH_2$ in ethanol + DI water mixture (1:1, v/v) g) $LDMH_2$ in the presence of 1 equiv. Zn(II) pH ≅ 7 h)$LDMH_2$ in the presence of 1 equiv. Zn(II) pH = 3

Fig. 11. Selectivity of LH_2 and $LDMH_2$ for Zn(II) in the absence or presence of other metal ions (stock $[LH_2] = [LDMH_2] = 2.0\times10^{-4}$ M in ethanol, stock $[Zn^{2+}] = 2.0\times10^{-5}$ M in DI water, stock $[Na^+] = [K^+] = [Mg^{2+}] = [Ca^{2+}] = [Al^{3+}] = [Cr^{3+}] = [Mn^{2+}] = [Hg^{2+}] = [Fe^{3+}] = [Co^{2+}] = [Ni^{2+}] = [Cu^{2+}] = [Cd^{2+}] = [Pb^{2+}] = 2.0\times10^{-3}$ M in DI water, λ_{Ex} = 350 nm, pH ≅ 7)

Fig. 12. Fluorescence intensity of a) LH_2 b) $LDMH_2$ as a function of Zn(II) concentration (1:1 v/v, stock [ligand] = 2.0×10^{-5} M in ethanol, stock $[Zn^{2+}] = 2.0\times10^{-4}$ M in DI water, λ_{Ex} = 350 nm, λ_{Em} = 446 nm)

Fig. 13. The color of a) LH_2-Zn and d)$LDMH_2$-Zn complexes under the fluorescence microscope with U-DM-DA/FI/TX2E filter. DNA comet assay images after electrophoresis of cells from chicken breast meat irradiated at b) 0.0 kGy LH_2-Zn staining c) 3.0 kGy LH_2-Zn staining e) 0.0 kGy $LDMH_2$-Zn staining and f) 3.0 kGy $LDMH_2$-Zn staining

Highlights

- Four Schiff base derivatives were investigated as a fluorescent sensor for Zn(II)
- The structure of the sensors are quite simple, one of them is commercially available
- Two chemosensors can selectively recognize Zn(II) ions over other important cations
- **Optimized methods** show **good linearity, precision, accuracy and low detection limits**
- Two chemosensors can be used as fluorescent **DNA staining agents**

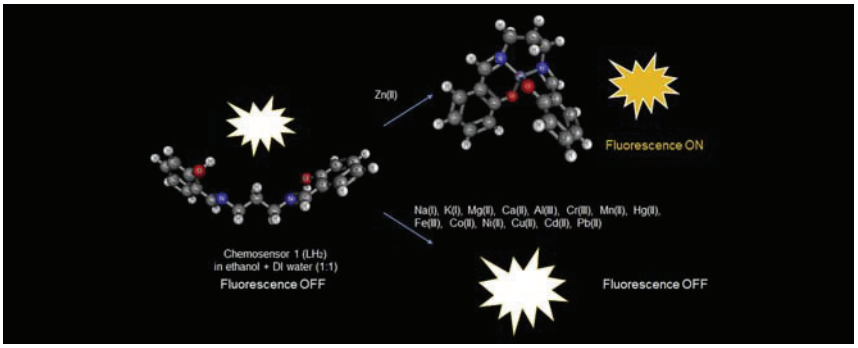

Graphics Abstract

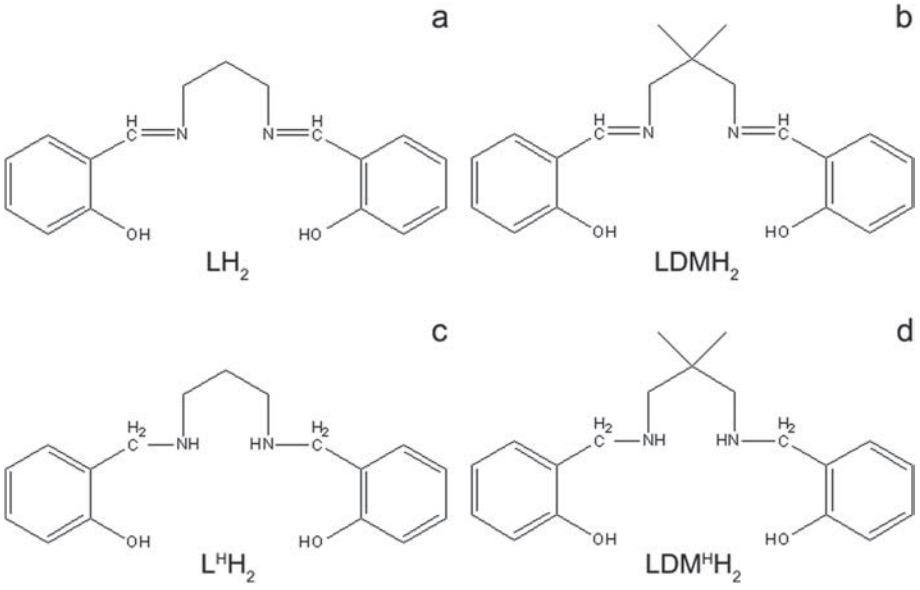

Figure 1

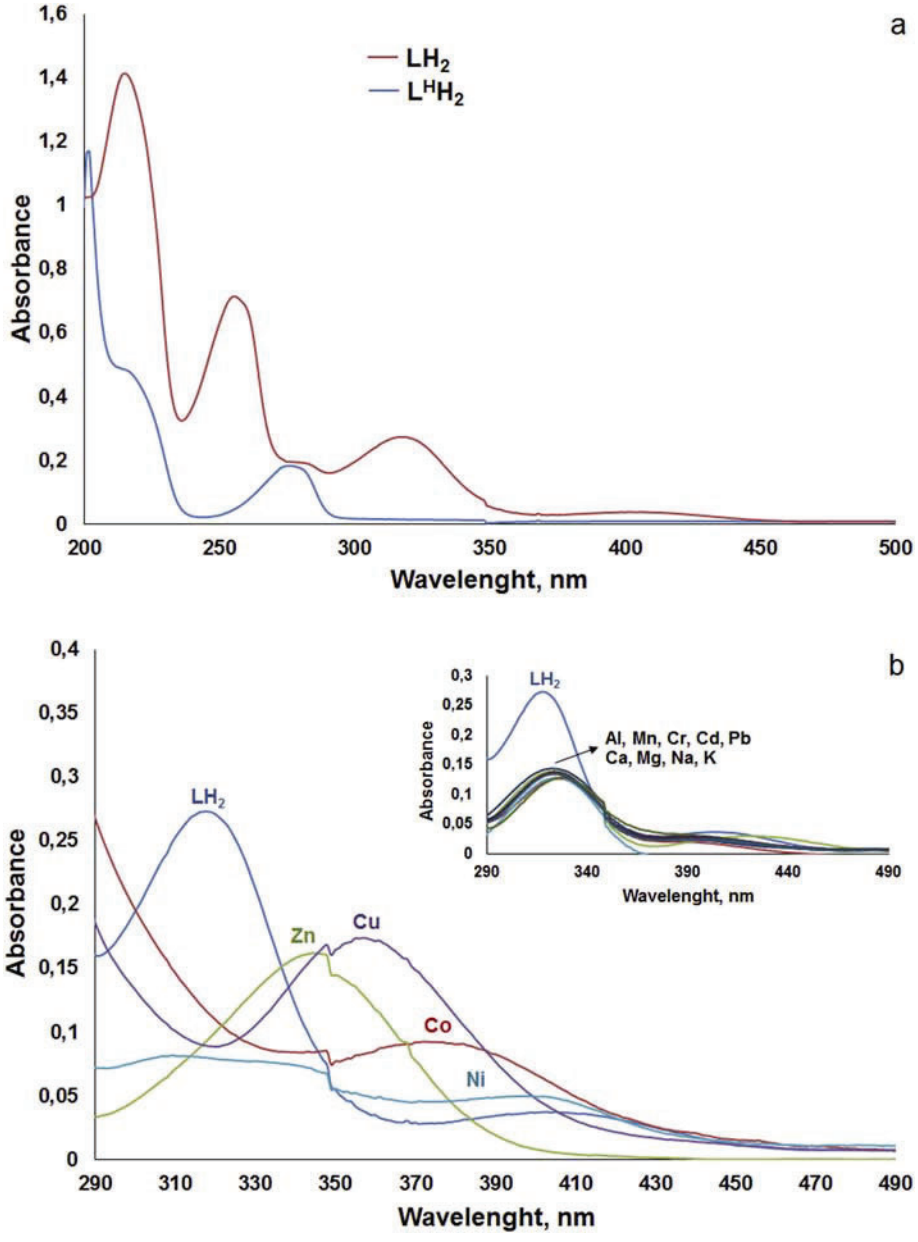
a
LH2
LHH2
Absorbance
Wavelenght, nm
b
LH2
Al, Mn, Cr, Cd, Pb
Ca, Mg, Na, K
Absorbance
Wavelenght, nm
Zn
Cu
Co
Ni
Absorbance
Wavelenght, nm

Figure 2

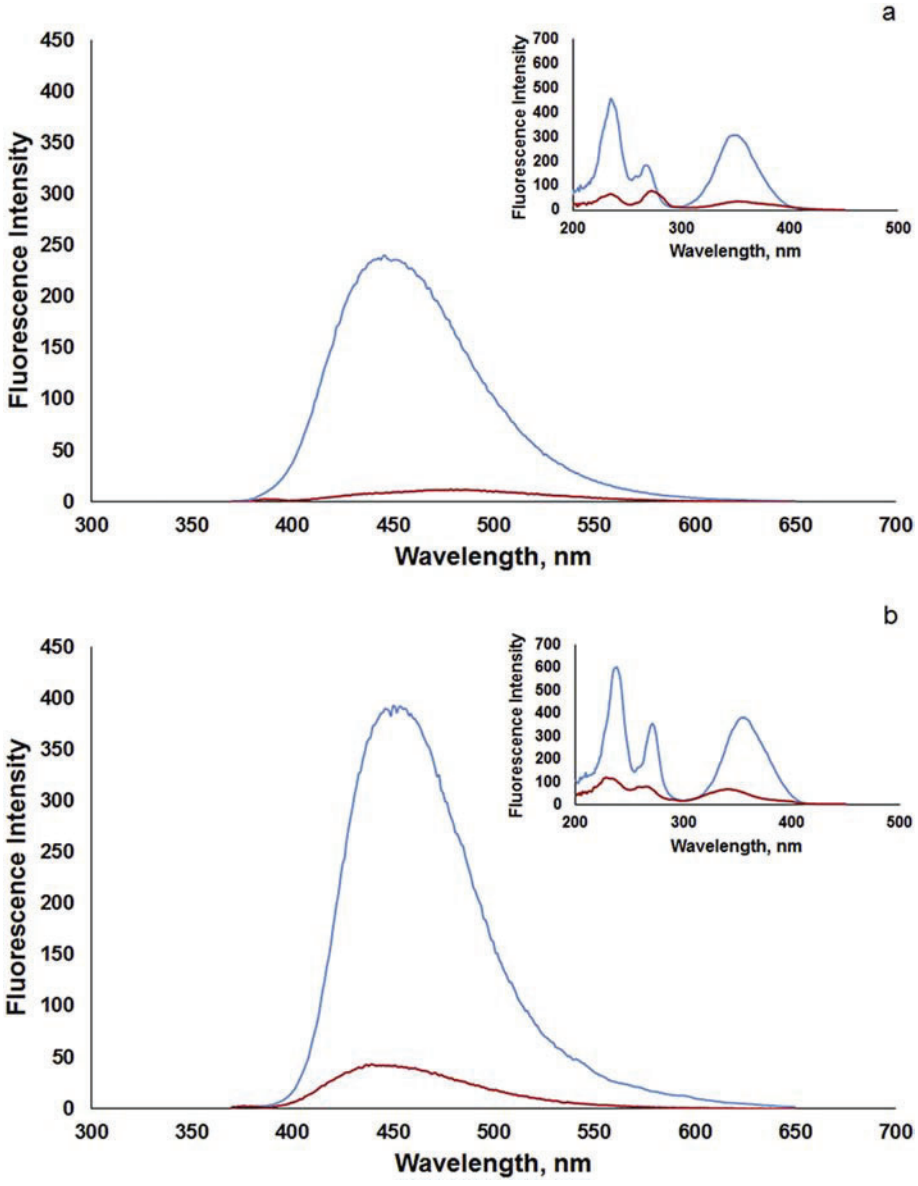
a
Fluorescence Intensity
Wavelength, nm
b
Fluorescence Intensity
Wavelength, nm

Figure 3

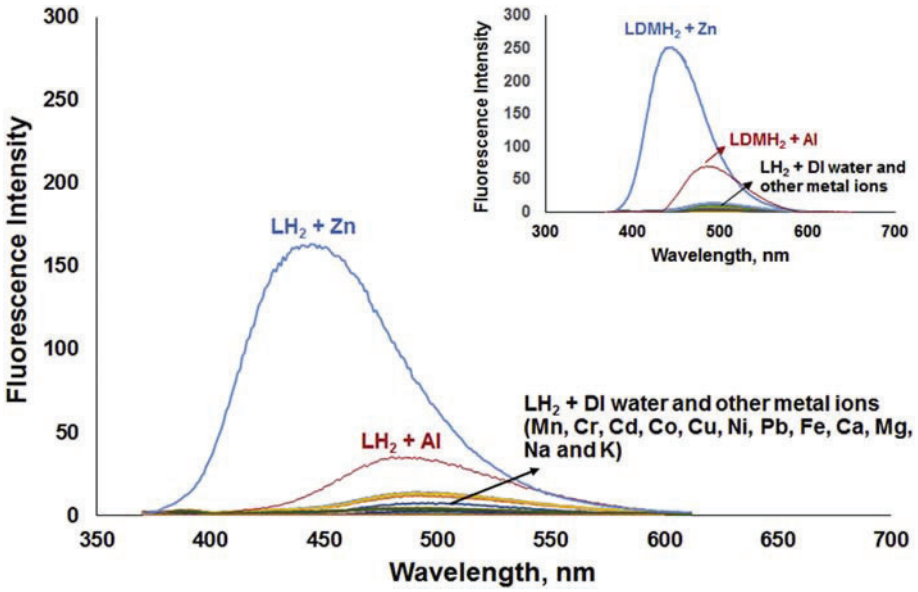
Fluorescence Intensity
Wavelength, nm
LH2 + Zn
LH2 + Al
LH2 + DI water and other metal ions (Mn, Cr, Cd, Co, Cu, Ni, Pb, Fe, Ca, Mg, Na and K)
LDMH2 + Zn
LDMH2 + Al
LH2 + DI water and other metal ions

Figure 4

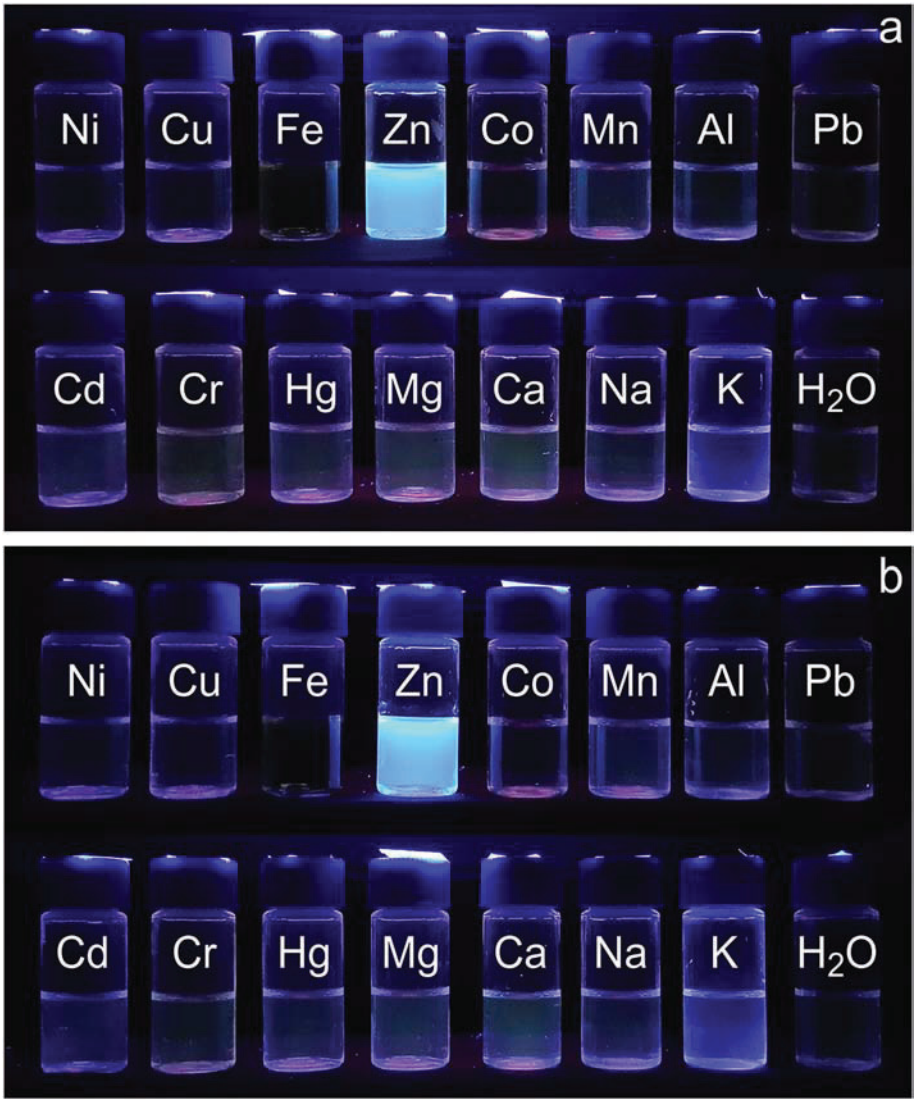
a
Ni
Cu
Fe
Zn
Co
Mn
Al
Pb
Cd
Cr
Hg
Mg
Ca
Na
K
H_2O
b
Ni
Cu
Fe
Zn
Co
Mn
Al
Pb
Cd
Cr
Hg
Mg
Ca
Na
K
H_2O

Figure 5

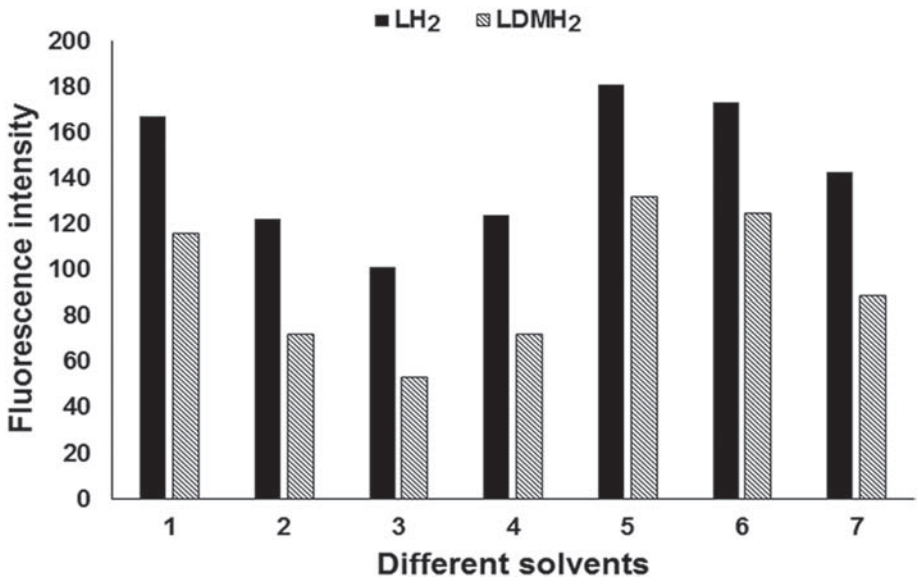
LH2
LDMH2
Fluorescence intensity
200
180
160
140
120
100
80
60
40
20
0
1
2
3
4
5
6
7
Different solvents

Figure 6

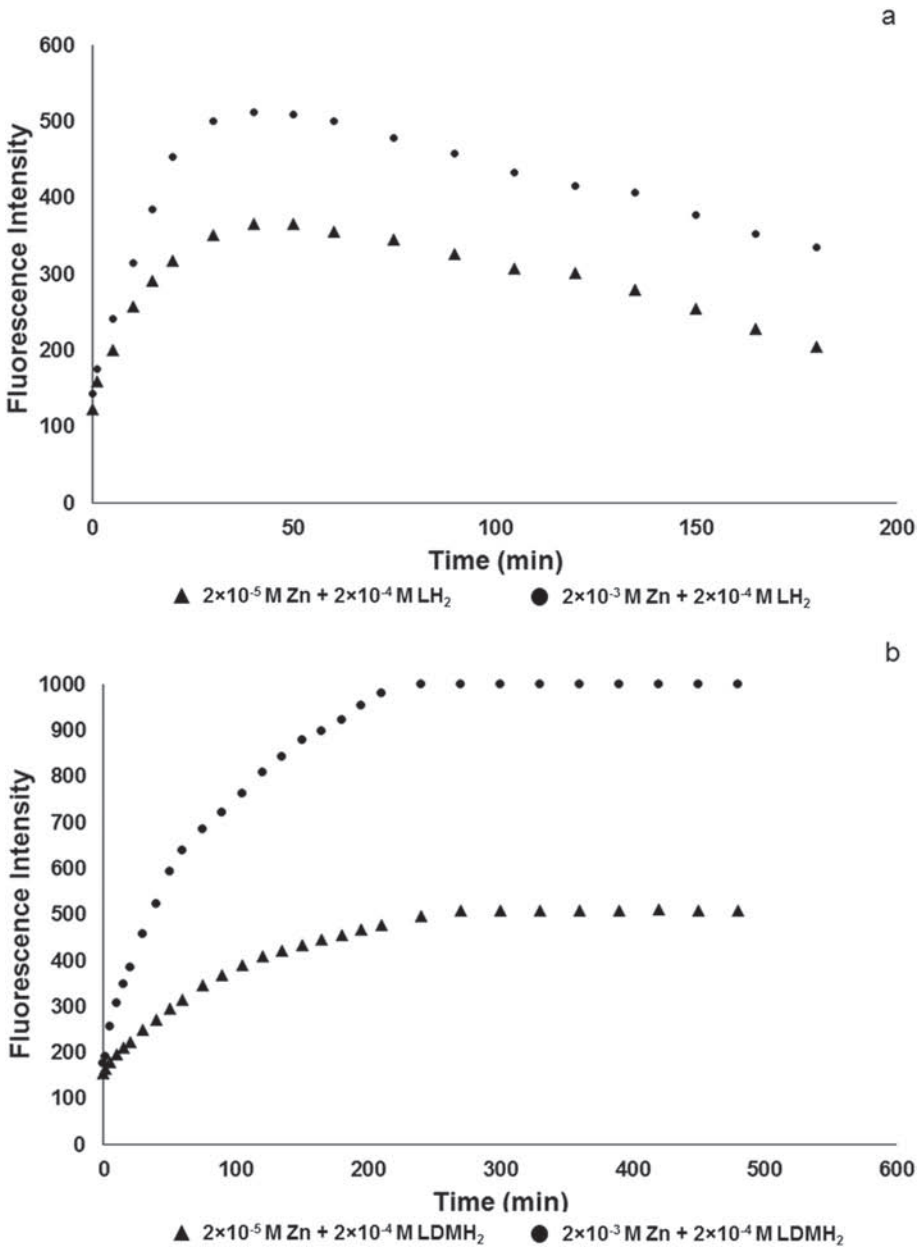
a
Fluorescence Intensity
600
500
400
300
200
100
0
0
50
100
150
200
Time (min)
▲ 2×10-5 M Zn + 2×10-4 M LH2
● 2×10-3 M Zn + 2×10-4 M LH2
b
Fluorescence Intensity
1000
900
800
700
600
500
400
300
200
100
0
0
100
200
300
400
500
600
Time (min)
▲ 2×10-5 M Zn + 2×10-4 M LDMH2
● 2×10-3 M Zn + 2×10-4 M LDMH2

Figure 7

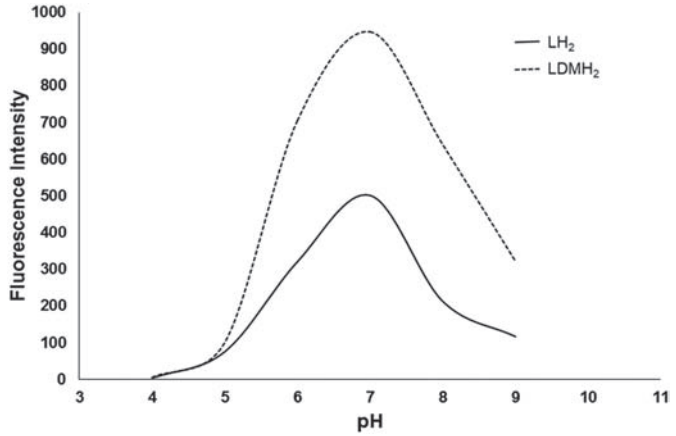
Fluorescence Intensity
1000
900
800
700
600
500
400
300
200
100
0
3
4
5
6
7
8
9
10
11
pH
LH2
LDMH2

Figure 8

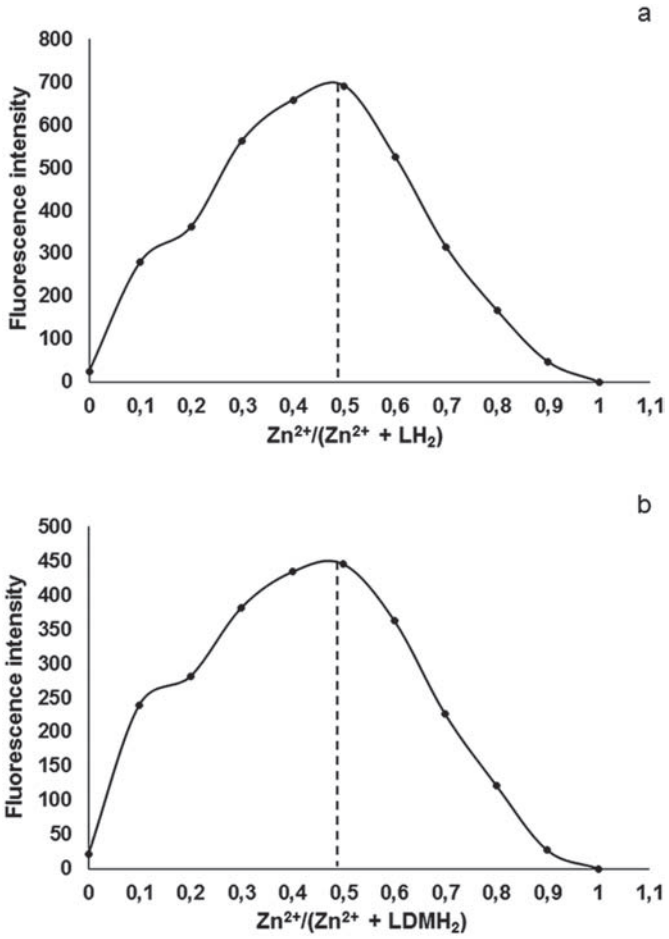
a
Fluorescence intensity
800
700
600
500
400
300
200
100
0
0 0,1 0,2 0,3 0,4 0,5 0,6 0,7 0,8 0,9 1 1,1
Zn2+/(Zn2+ + LH2)
b
Fluorescence intensity
500
450
400
350
300
250
200
150
100
50
0
0 0,1 0,2 0,3 0,4 0,5 0,6 0,7 0,8 0,9 1 1,1
Zn2+/(Zn2+ + LDMH2)

Figure 9

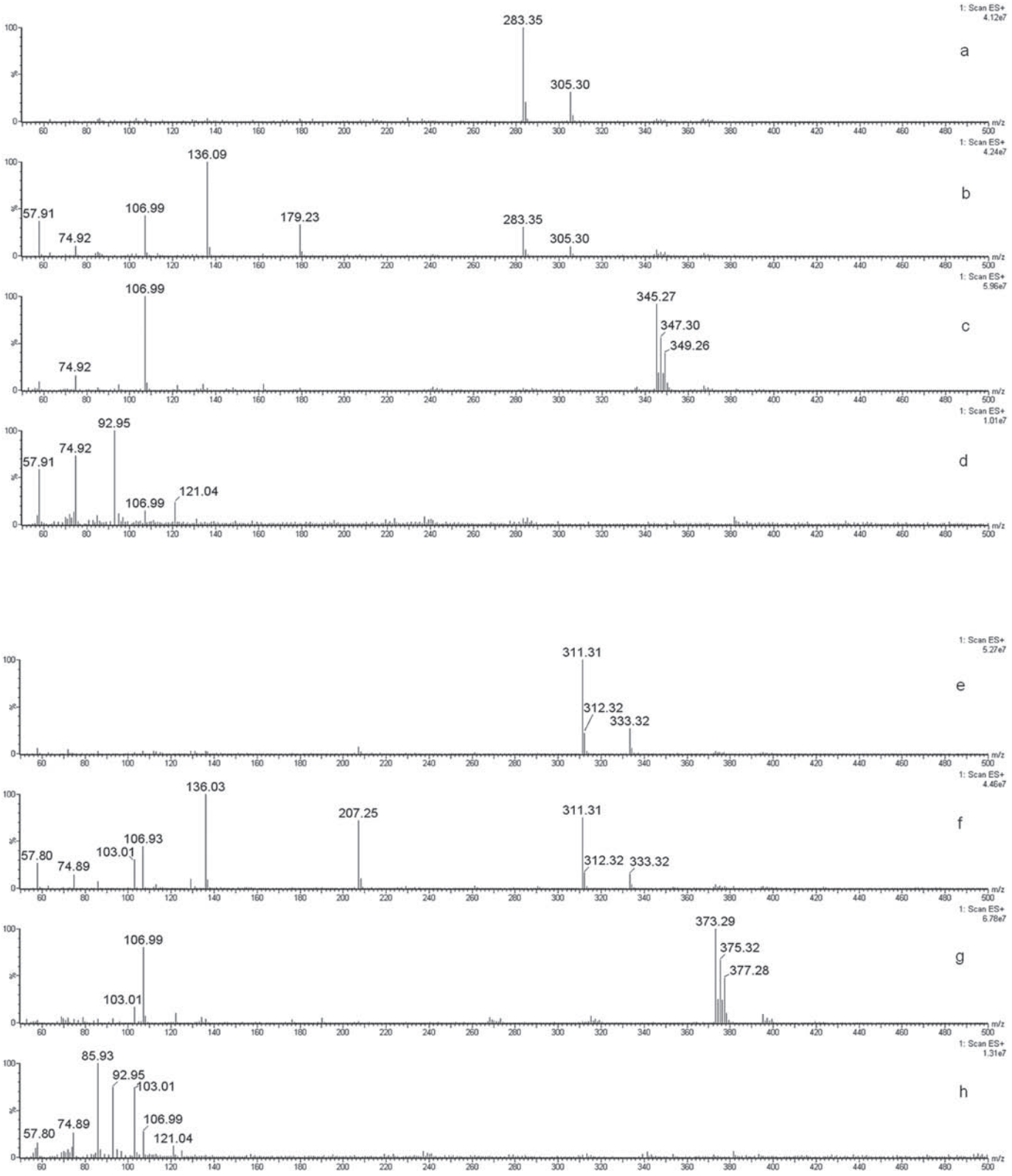
1: Scan ES+
4.12e7
283.35
305.30
a
1: Scan ES+
4.24e7
136.09
57.91
106.99
74.92
179.23
283.35
305.30
b
1: Scan ES+
5.96e7
106.99
345.27
347.30
349.26
74.92
c
1: Scan ES+
1.01e7
92.95
74.92
57.91
106.99
121.04
d
1: Scan ES+
5.27e7
311.31
312.32
333.32
e
1: Scan ES+
4.46e7
136.03
207.25
311.31
106.93
103.01
57.80
74.89
312.32
333.32
f
1: Scan ES+
6.78e7
373.29
106.99
375.32
377.28
103.01
g
1: Scan ES+
1.31e7
85.93
92.95
103.01
106.99
74.89
57.80
121.04
h
m/z

Figure 10

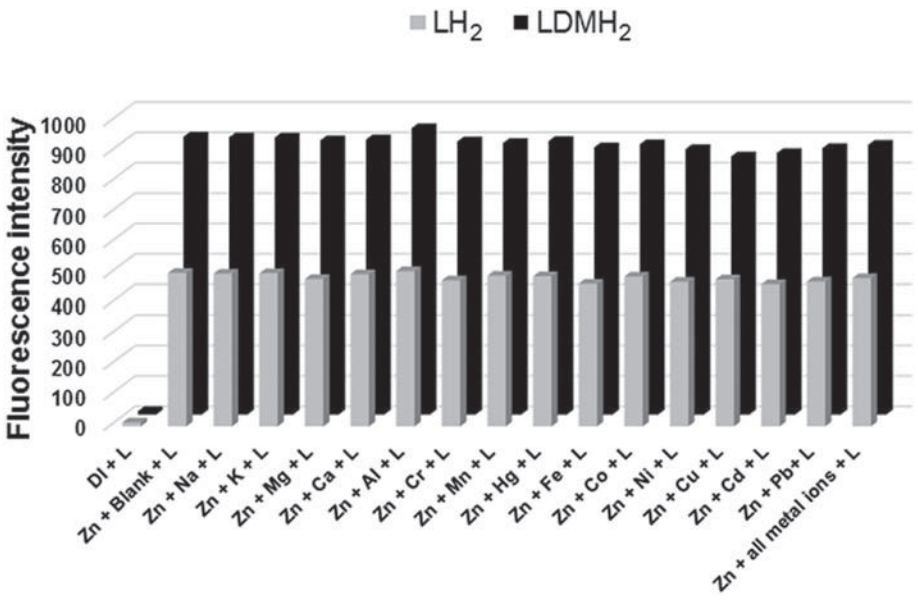
LH2
LDMH2
Fluorescence intensity
1000
900
800
700
600
500
400
300
200
100
0
DI + L
Zn + Blank + L
Zn + Na + L
Zn + K + L
Zn + Mg + L
Zn + Ca + L
Zn + Al + L
Zn + Cr + L
Zn + Mn + L
Zn + Hg + L
Zn + Fe + L
Zn + Co + L
Zn + Ni + L
Zn + Cu + L
Zn + Cd + L
Zn + Pb+ L
Zn + all metal ions + L

Figure 11

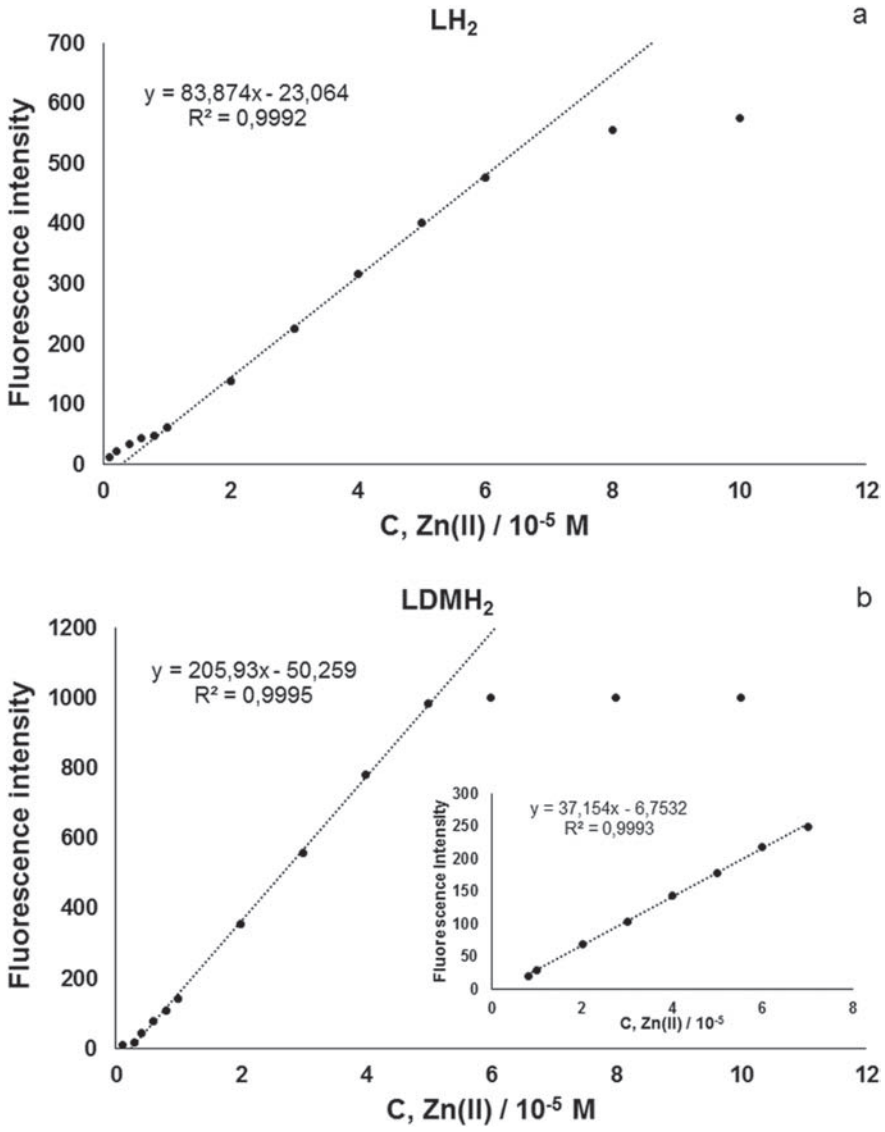
a
LH2
y = 83,874x - 23,064
R² = 0,9992
Fluorescence intensity
C, Zn(II) / 10-5 M
b
LDMH2
y = 205,93x - 50,259
R² = 0,9995
y = 37,154x - 6,7532
R² = 0,9993
Fluorescence Intensity
C, Zn(II) / 10-5
Fluorescence intensity
C, Zn(II) / 10-5 M

Figure 12

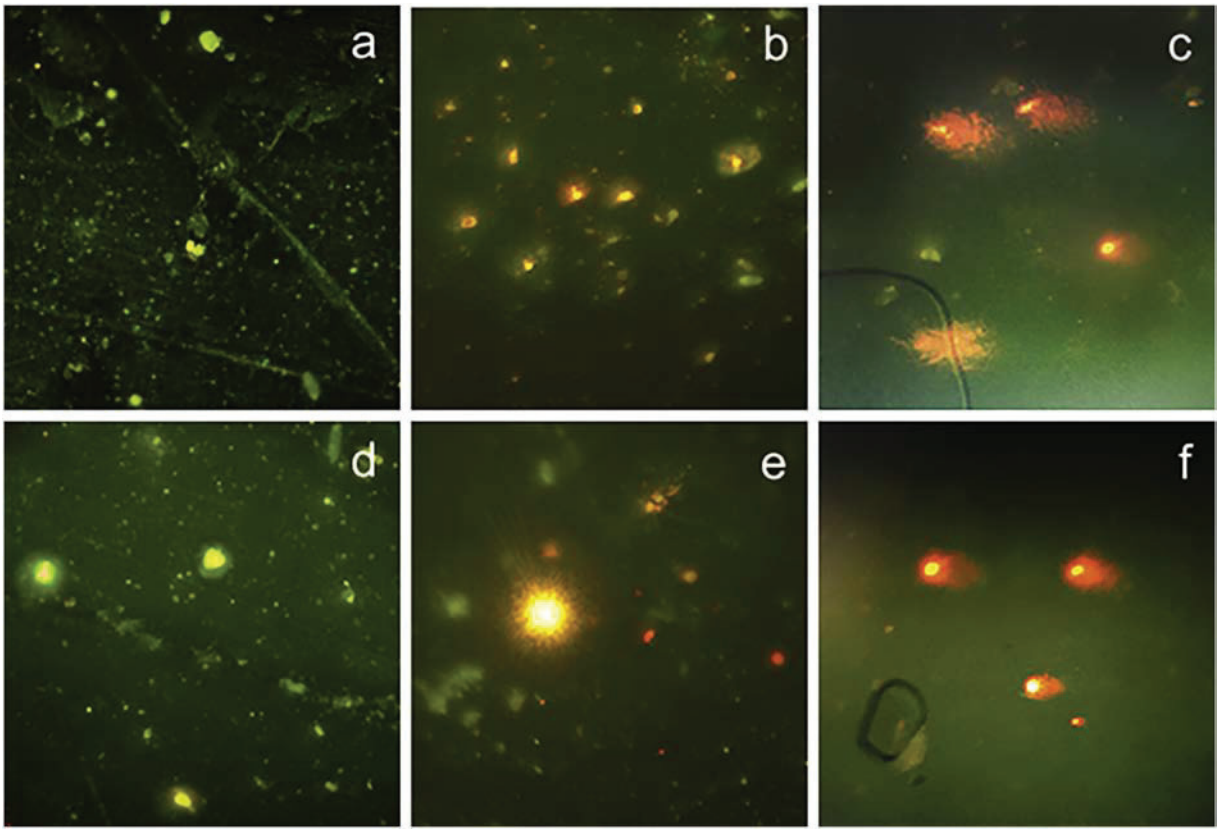

Figure 13